ACOUSTIC EMISSION INSPECTION AND ANALYSIS OF CRIMPED METAL-COMPOSITE JOINTS SUBJECTED TO BENDING

Alain Prenleloup, Thomas Gmür*, John Botsis
Ecole polytechnique fédérale de Lausanne (EPFL), School of Engineering (STI),
EPFL – STI – LMAF, Bâtiment ME, Station No 9, 1015 Lausanne, Switzerland

Konstantin O. Papailiou, Kurt Obrist
Pfisterer-Sefag AG, Werkstraße 7, 6102 Malters, Switzerland

Philippe Bonhôte
Haute Ecole d'Ingénierie et de Gestion du Canton de Vaud (HEIG-VD), HEIG-VD – TIN,
Route de Cheseaux 1, 1401 Yverdon, Switzerland

Abstract

Experimental and numerical studies are carried out on crimped mixed metal-composite joints integrated in electrical insulators subject to bending. Strain monitoring is performed with strain gauges and a six-channel acoustic emission equipment to shed light in the process of damage until failure and several 3D nonlinear finite element models are constructed to compare the experimental results in strains and damage with the numerical predictions. Excellent agreement is found between the two sets of data and the different damage mechanisms observed are reported.

Keywords: Acoustic emission, Metal-composite joint, Finite element method, Composite insulators

1. Introduction

In comparison to single-material components, mixed metal-composite structural elements exhibit differences in the constitutive law, thermal or hydrothermal response and failure characteristics between the metal and the composite. This introduces zones of high stresses that induce damage initiation and growth, leading to fracture onset and ultimately failure. Consequently, in order to use such composite-metal joints in an optimal way, a thorough characterization of their mechanical and failure behaviour is required. Among the different issues concerning the reliability of these joints, the distribution of the stresses in the joint, the efficiency of the interface between the metal and the composite, and the fatigue and fracture of the composite under different external mechanical loads are considered very important.

Mixed composite-metal joints are increasingly used in industrial equipments such as automotive, aircraft, aerospace or electrical components. As a specific application of mixed joints encountered in high-voltage networks, silicon composite insulators with crimped metal end-fittings manufactured for high-voltage transmission lines or substations are now replacing conventional porcelain elements due to the hydrophobic nature of their silicon surface, their insensitiveness to dynamic loads such as short-circuits or earthquakes, and their light weight compared to porcelain which facilitates their handling, transport and installation. These structures, however, require two metal end-fittings in order to transfer loads from the high-voltage conductor to the tower or the substation equipment. Two different designs are adopted according to whether the insulator is loaded primarily in bending or in traction. In the first case, the insulator is chosen tubular with aluminium fittings bonded to the composite tube with an epoxy adhesive layer. In the second situation, a thin rod-type insulator is preferred where steel end-

* Corresponding author : Thomas Gmür (thomas.gmuer@epfl.ch)

fittings are crimped to the composite rod with a radial compression by means of a hydraulic press until a sufficient plastic deformation is initiated in the metal. Due to the lower assembly cost of the latter solution, the crimping strategy is nowadays also applied to thick rod-type insulators (with generally a diameter above 50 mm) subject to bending.

Only a few papers have been published on the stress and failure analysis of composite insulators consisting of a glass-reinforced polymer rod with two metal end-fittings radially crimped onto the composite during assembly. In these works, numerical non-linear studies and experimental investigations are performed on non-adhesively bonded joints under axial tensile loads [1–9] or being subjected to corrosion by moisture absorption [10–14]. On the mechanical point of view, no investigations have been conducted so far on the bending behaviour of crimped rod-type insulators. According to the limited current research and development in this field, a systematic and integrated approach that would account for different types of configurations and lead to realistic design methodology for crimped composite-metal structural joints subject to bending is desirable. The present paper is aimed at a critical evaluation of the bending behaviour of specific steel-glass/epoxy crimped joints used in thick-rod composite insulators connecting transformers and substations to overhead lines up to the highest voltage levels. Numerical simulations of the stress distributions throughout the joints are performed by means of full 3D finite element models. The distributions of the internal stresses are investigated and the different damage mechanisms of the insulator are identified. An experimental setup based upon acoustic emission and strain gauges is also developed in order to validate the numerical models and to follow, up to failure, the damage progress in the joints. This work should serve as a basic step towards the optimization of the mechanical bearing capacity of thick-rod insulators subject to bending.

2. Description of the crimped joints investigated

Manufactured by Pfisterer-Sefag® (Switzerland), the thick rod-type composite insulators investigated in this study are made of an epoxy rod reinforced with ECR-glass fibres and of two steel fittings strongly crimped to both ends of the rod (Fig. 1). For preventing degradation in corrosive environments and electrical leakage currents, the composite is covered with a silicone rubber housing or shed which is not considered in the analysis.

The composite core, obtained by a pultrusion technique, is a unidirectional glass reinforced polymer (GRP) rod. The matrix is made of epoxy resin and the average volume fraction of the glass fibres is measured as 56%. Geometrically, the rod considered has a nominal diameter between 51 and 88 mm and a length, adjustable to customer's need, ranging typically from 0.4 to 2.0 m. Tempered unalloyed carbon steel is chosen for the metal end-fittings fabricated directly by the manufacturer of the insulators. Also achieved by the manufacturer, the crimping of the end-fittings on the composite rod is performed by means of a hydraulic press. A high internal pressure, inducing a radial shortening of the steel adherends during crimping, is required in order to reach a predefined value, depending on the diameter of the rod, for the shortening after relaxing the crimping pressure.

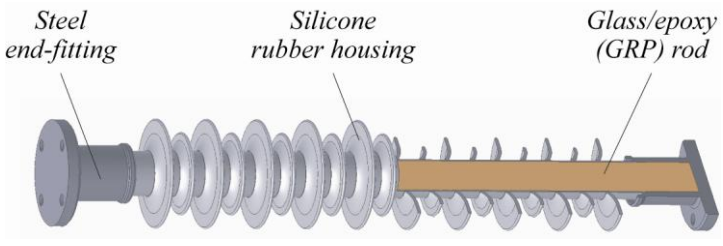

Figure 1 : Composite insulator

The values of the constitutive parameters for the epoxy resin and the ECR-glass fibres have been chosen in the literature. By using the classical rule of mixtures applied to the whole homogenized GRP core and knowing the volume fraction of the fibres, the elastic properties of the unidirectional composite rod could be easily estimated. Some of these evaluated properties have been corroborated with the values provided by the supplier of the composite rod and have been confirmed with a normalized tensile test performed on an in-house axial/torsion testing system. The latter has also been used for determining the elastic and plastic constitutive parameters of the steel end-fittings. The properties found for the different materials are listed in Table 1.

Table 1 Material properties (engineering constants)

Component	E_1[a] (GPa)	E_2, E_3 (GPa)	G_{23} (GPa)	G_{31}, G_{12} (GPa)	ν_{23} (–)	ν_{31}, ν_{12} (–)
Press jaw	207	–	–	–	0.29	–
End-fitting	200	–	–	–	0.29	–
Rod	44	10.3	4.3	5.1	0.5	0.32

[a] For the composite, subscripts 1, 2 and 3 refer to the fibre- and both transverse-directions

3. Experimental setup

Applying a transverse load at the free end of a built-in insulator, a specific experimental setup has been developed for the analysis of the composite-metal joint under bending. Based upon a servo-hydraulic test frame provided by the manufacturer of the insulators, the system is equipped with a hydraulic jack and a load cell, and instrumented with an LVDT (linear variable differential transformer) displacement transducer, six resistive strain gauges pasted at different locations on the composite rod and the outer surface of the fixed end-fitting and a six-channel acoustic emission system to shed light in the process of damage activity on the joint as a function of the bending moment (Fig. 2).

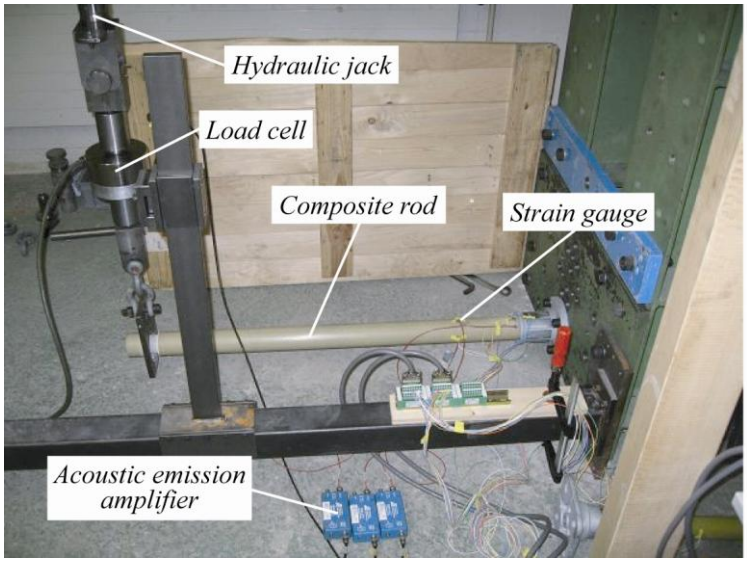

Figure 2 : Experimental setup

4. Finite element modelling

Full 3D solid finite element models of the different joints have been constructed using the commercially available ABAQUS® software. By symmetry, only a half of the complete joint is modelled (Fig. 3). Non-linear simulations are performed successively on the 51 to 88mm-thick composite insulators for the three following steps: the crimping of the end-fitting onto the composite rod, the relaxation of the crimping pressure and the bending of the entire joint.

The numerical models are based upon hexahedral quadratic 20-node solid elements with a reduced integration scheme for the computation of the structural components (C3D20R in the ABAQUS® element nomenclature). The mesh is composed of 112 finite elements per hardened steel jaw or blade (not represented in Fig. 3) compressing the end-fitting on the composite rod, 4915 elements for the steel half-fitting and 6912 elements for the composite half-cylinder. As illustrated in Fig. 3, the grid for the composite rod is refined at the outlet of the end-fitting since this zone is subject to stress concentrations during the bending phase as shown in the next subsections.

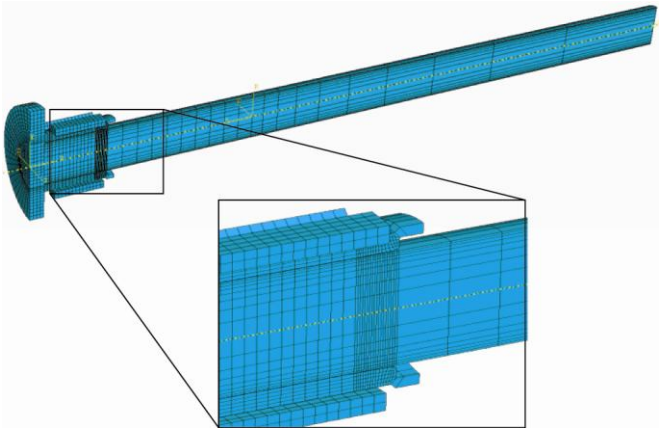

Figure 3 : Finite element model of a 63mm-thick insulator

For the crimping step, a Coulomb contact law with a friction coefficient of 0.35, corresponding to the mean value of data measured on several specimens, is adopted in the models for simulating the contact at the interfaces between the press and the fitting and between the latter and the rod. For the bending step, a full damage tensor criterion (similar to the Tsai-Wu criterion) is applied to the elastic transversely isotropic composite. Derived from in-house performed axial tensile and compression, in-plane shear and torsion, and biaxial compression strength tests on specimens cut in rods of various diameters, ultimate longitudinal strengths in tension and compression are measured as 1038 and –794 MPa, respectively, and the corresponding transverse strengths are found as 32 and –141 MPa. Values of 54 and –500 MPa are obtained for the ultimate longitudinal-transverse shear strength and the radial ultimate strength.

5. Numerical and experimental stress analysis

It can be shown that, contrary to the situation inherent in thin composite insulators subject to tensile loading [8,9], the crimping process is not critical for thick insulators. Since these structures are primarily designed for resisting to bending moments caused by loads mainly orthogonal to the longitudinal axis, the crimping pressure is chosen sufficiently low to avoid any damage of the composite rod. The stress analysis is thus focused here on the behaviour of the insulators during the bending phase.

The ultimate mechanical loading of 15 kN (measured experimentally) is applied to the 51mm-thick model at its free end. Located at the outlet of the end-fitting on the outer compressive fibre of the rod, a maximum longitudinal normal stress σ_{zz} of –1320 MPa is then obtained in the composite, while a maximum radial-axial shear stress τ_{rz} of 131 MPa is predicted on the axis of the composite rod in the middle of the end-fitting (Fig. 4). The 63mm-thick insulator is subject to the ultimate mechanical loading of 20 kN. The corresponding maximum longitudinal normal stress σ_{zz} and radial-axial shear stress τ_{rz} are equal to –1330 and 123 MPa, respectively, and are observed at the same relative locations than for the thinner rod (Fig. 4). It is also seen that the stress distributions are very similar for both insulators. Furthermore, it could be shown that outside the bond the normal and shear stresses follow exactly the linear and constant analytical predictions given by the strength-of-materials theory for a cantilever beam subject to bending with shearing. The results obtained with an 88mm-thick insulator are not shown here since they are in essence identical to the former ones.

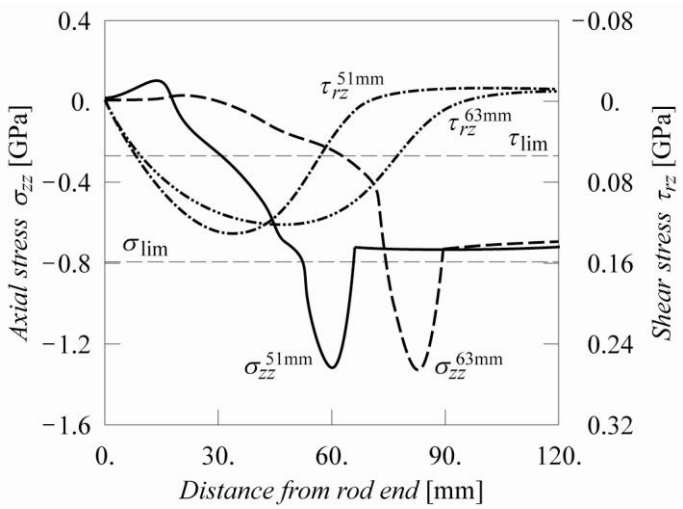

Figure 4 : Numerical stress distributions in the composite rod at the ultimate loading

The simulated load-displacement curves (applied load at the free end of the insulator versus deflection at the LVDT location) for both the 51 and 63mm-thick insulators are compared in Fig. 5 with the corresponding experimental data (three specimens have been tested for each diameter). An excellent agreement between the two sets of results can be observed in the nearly linear behaviour range of the experiments. It could also be shown that in this range the numerical strain predictions fully agree with the measurements derived from the strain gauges. However, the onset of nonlinearity in the load-displacement curves suggests that a local damage is initiated in the composite rod at 50 to 60% of the maximum mechanical loading, which is confirmed in Fig. 4 where locally the values of the normal and shear stresses predicted exceed the ultimate compression and shear strengths σ_{lim} and τ_{lim}, respectively.

6. Numerical and experimental failure analysis

Expressed in the form of a normalized index (stress ratio) corresponding to the inverse of the factor by which the applied bending load can by linearly magnified before failure, the results found for the damage criterion when subjecting the 51mm- and 63mm-thick insulators to the ultimate mechanical loading is illustrated in Fig. 6a. It can be observed that the damage index exceeds the unit limit value in the middle of the composite rod, where the shear stresses are dominant, and in the vicinity of the two

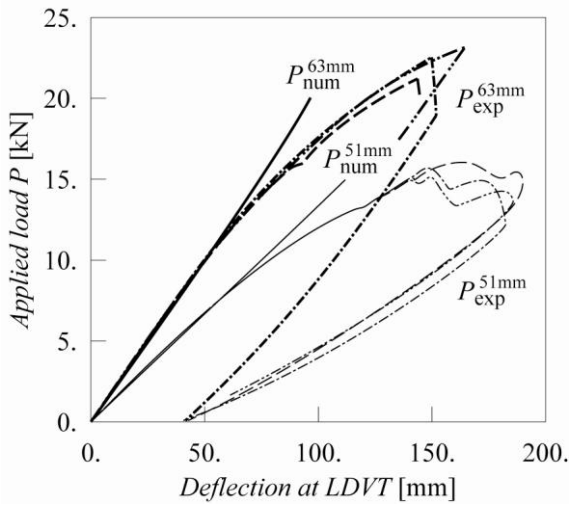

Figure 5 : Numerical and experimental load-displacement curves for the insulators investigated

contact points with the end-fitting, subjected to high radial stresses and located at the beginning of the rod for the part of the composite under tension and at the bond end for the part in compression. By decreasing the intensity of the applied load to 60 and 50% of the ultimate mechanical loading for the 51mm- and 63mm-thick insulators respectively, the damage index can be reduced so that the critical unit value is exceeded only very locally (Fig. 6b). It can be noticed that the reduced loads correspond precisely with the onset of nonlinearity in the load-displacement curves shown in Fig. 5. It should also be mentioned that at this loading intensity only local damage is initiated, which explains that the mechanical bearing capacity of these insulators is much higher.

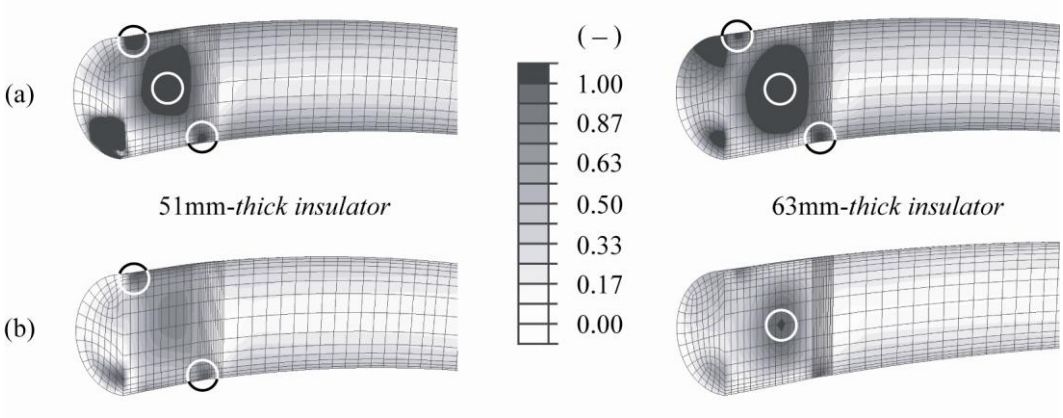

Figure 6 : Damage index for the 51mm- and 63mm-thick insulators (a) at the ultimate mechanical loading and (b) at 60 or 50%, respectively, of this load (a circle indicates highest index location)

The initiation of the local damage can be highlighted by means of the abovementioned experimental device. Several 51mm-, 63mm- and 88mm-thick insulators have been loaded up to failure of the metal-composite joint and the progress of the damage activity has been measured with the acoustic emission equipment. The intensity (number of counts and so-called acoustic emission energy averaged over 5 seconds) of the measured acoustic emission activity in function of the bending load applied according to a protocol fixed by IEEE standards is shown in Fig. 7 for the 51mm- and 63mm-thick insulators. It is apparent that the first slight acoustic emission activity appears for both insulators at the

respective onset of nonlinearity in the load-displacement curves (Fig. 5). A severe activity, corresponding to the perturbation observable in the nonlinear range of the load-displacement curves, can be seen when the applied load is increased again after the plateau imposed by the loading protocol and the intensity of the acoustic emission raises a maximum at the ultimate mechanical loading.

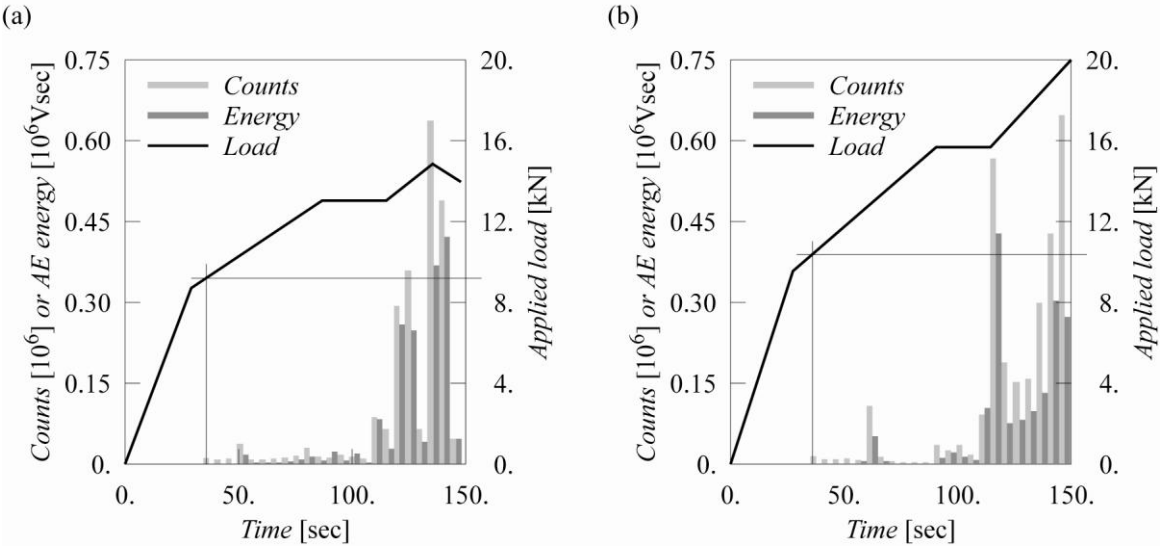

Figure 7 : Acoustic emission (AE) activity during bending of the (a) 51mm- and (b) 63mm-thick insulators

The damage mechanism for the 51mm-thick composite rod is illustrated in Fig. 8a, where it can be observed that failure is caused by a transverse crack propagation due to the normal stresses in the compressive part of the rod. This phenomenon is to be related with the damage index shown in Fig. 6b which reaches its highest value precisely in the zone near the initiation of the transverse cracks. For the 63mm- and 88mm-thick insulators, a longitudinal crack propagation due to the shear stresses in the centre of the rod occurs in addition to the transverse crack propagation, as shown in Fig. 8b. This observation is again confirmed by the distribution of the damage index in Fig. 6b, where it is seen that a second critical failure area appears in the middle of the thicker composites.

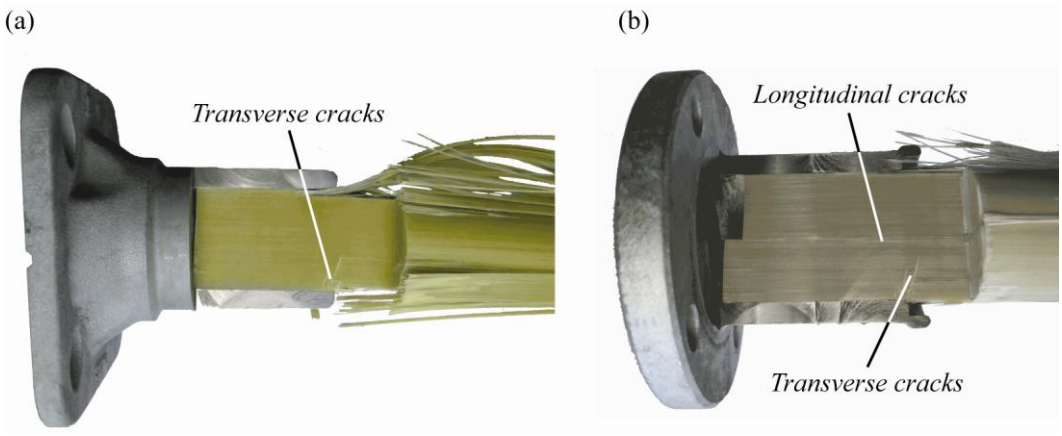

Figure 8 : Damage mechanisms for the (a) 51mm- and (b) 63mm-thick insulators

7. Conclusions

Experimental tests and numerical simulations have been performed on crimped metal-composite insulators subject to bending. The investigations have highlighted the complexity of the nonlinear stress state in the composite rod and have illustrated the different damage mechanisms (longitudinal or transverse crack propagation) that may occur together or separately.

Acknowledgments

The authors wish to acknowledge the financial support from the Swiss Commission for Technology and Innovation under grant CTI 6798.1.

References

[1] Bansal, A., Schubert, A., Balakrishnan, M.V., Kumosa, M. (1995), Finite element analysis of sub-station composite insulators, *Compos Sc Technol*, **55**, No.4, pp. 375–389.
[2] Lanteigne, J., Lalonde, S., de Tourreil, C. (1996), Optimization of stresses in the end-fittings of composite insulators for distribution and transmission lines, *J Reinf Plast Compos*, **15**, No.6, pp. 467–478.
[3] Bansal, A., Kumosa, M. (1997), Mechanical evaluation of axially loaded composite insulators with crimped end-fittings, *J Compos Mater*, **31**, No.20, pp. 2074–2104.
[4] Kumosa, M., Han, Y., Kumosa, L. (2002), Analyses of composite insulators with crimped end-fittings : Part I – Non-linear finite element, *Compos Sc Technol*, **62**, No.9, pp. 1191–1207.
[5] Kumosa, M., Armentrout, D., Kumosa, L., Han, Y., Carpenter, S.H. (2002), Analyses of composite insulators with crimped end-fittings : Part II – Suitable crimping conditions, *Compos Sc Technol*, **62**, No.9, pp. 1209–1221.
[6] Mobasher, B., Kingsbury, D., Montesinos, J., Gorur, R.S. (2003), Mechanical aspects of crimped glass reinforced plastic (GRP) rods, *IEEE Trans Power Delivery*, **18**, No.3, pp. 852–858.
[7] Duriatti, D., Béakou, A., Levillain, R. (2006), Optimisation of the crimping process of a metal end-fitting onto a composite rod, *Compos Struct*, **73**, No.3, pp. 278–289.
[8] Prenleloup, A., Gmür, T., Botsis, J., Papailiou, K.O. (2006), Acoustic emission study and strength analysis of crimped steel-composite joints under traction, *Compos Struct*, **74**, No.3, pp. 370–378.
[9] Prenleloup, A., Gmür, T., Bonhôte, P., Botsis, J., Papailiou, K.O. (2006), Experimental and numerical strength analysis of mixed metal-composite crimped or adhesively bonded joints, *Proc 3rd Int Conf Compos Testing Model Identification CompTest 2006*, pp. 25–26.
[10] Kumosa, L., Benedikt, B., Armentrout, D., Kumosa, M. (2004), Moisture absorption properties of unidirectional glass/polymer composites used in composite (non-ceramic) insulators, *Compos A: Appl Sc Manufact*, **35**, No.9, pp. 1049–1063.
[11] Kumosa, M., Kumosa, L., Armentrout, D. (2005), Failure analyses of nonceramic insulators : Part I – Brittle fracture characteristics, *IEEE Elec Insulation Mag*, **21**, No.3, pp. 14–27.
[12] Kumosa, M., Kumosa, L., Armentrout, D. (2005), Failure analyses of nonceramic insulators : Part II – The brittle fracture model and failure prevention, *IEEE Elec Insulation Mag*, **21**, No.4, pp. 28–41.
[13] Gorur, R.S., Mobasher, B., Kumosa, M., Kumosa, L., Armentrout, D. (2005), Can water cause brittle fracture failures of non-ceramic insulators in the absence of electric field, *IEEE Trans Dielec Elec Insulation*, **12**, No.3, pp. 621–626.
[14] Kumosa, L.S., Kumosa, M.S., Armentrout, D.L. (2005), Resistance to brittle fracture of glass reinforced polymer composites used in composite (nonceramic) insulators, *IEEE Trans Power Delivery*, **20**, No.4, pp. 2657–2666.